Modeling of Anthropogenic Heat Flux Using HJ-1B Chinese Small Satellite Image: A Study of Heterogeneous Urbanized Areas in Hong Kong

Man Sing Wong, Jinxin Yang, Janet Nichol, Qihao Weng, Massimo Menenti, and PW Chan

***Abstract*—Anthropogenic heat is the heat flux generated by human activities and is a major contributor to the formation of an urban heat island. In a city such as Hong Kong, obtaining pure pixels from medium- or coarse-resolution remote sensing images is challenging. Considering the completely different thermal properties of vegetation and impervious surfaces, this letter developed a novel algorithm to estimate anthropogenic heat fluxes by decomposing image pixels into fractions of impervious surfaces and vegetation, and by estimating the total heat flux for the mixed pixel. The Chinese small satellite HJ-1B images with a spatial resolution of 30 and 300 m for visible and thermal wavebands, respectively, and the temporal resolution of four days were used for the heat flux modeling. Results show that anthropogenic heat fluxes in Hong Kong are correlated to the building density and the building height, with $r^2 = 0.92$ and 0.58 on October 11, 2012 and $r^2 = 0.94$ and 0.62 on January 13, 2013, respectively. The average anthropogenic heat fluxes in urban areas are 289.16 and 283.17 W/m^2 on October 11, 2012 and on January 13, 2013, respectively, and the commercial areas emit the largest anthropogenic heat fluxes around 500–600 W/m^2 compared with other land-use types. The derived anthropogenic heat fluxes can help in planning and environmental authorities to pinpoint "hot-spot" areas, and they can be used for compliance monitoring.**

***Index Terms*—Energy balance model, heat flux, mixed pixel, small satellite, urban areas.**

I. Introduction

ANTHROPOGENIC heat is comprised of the heat discharged from space heating and cooling, industrial plants, vehicle exhausts, and human metabolism, and it is a major contributor to urban heat island (UHI) formation. In cities, this heat typically contributes 15–50 W/m^2 to the local heat balance and several hundred watts per square meter in the center of large cities in cold climates, and it is expected to exceed 400–1500 W/m^2 in the center of Tokyo [3]. The estimation of anthropogenic heat generation can be determined by: 1) *in situ* measurements, which determine heat fluxes at the building level [14], [20]; 2) numerical modeling, which uses spatial information, e.g., energy consumption, population, and traffic data [3], [6], [7], [16], [21]; and 3) remote sensing techniques coupled with satellite, geographic information system, and meteorological data [4], [22], [24]. However, *in situ* measurements and numerical models are highly restricted by data availability, and they are labor and computer intensive. Remote sensing techniques are alternatives to estimate anthropogenic heat, [4], [5], [17], but they are not yet adequately refined. In remote sensing studies, the energy balance model has been proposed to retrieve the anthropogenic heat flux over a large area. A comprehensive review of the energy balance model was given in [2] and [13]. However, many studies of satellite-derived air and land-surface temperatures have been conducted [9], [15], but there are still few attempts to derive anthropogenic heat fluxes using satellite images. The work in [25] developed a semitheoretical estimation of heat fluxes using satellite data. Kato and Yamaguchi [4] developed a method to separate the anthropogenic heat flux from the sensible heat flux, and they modified their method to retrieve anthropogenic heat as the residual in the heat balance model [5]. In these studies, heat fluxes are not generated from remote sensing data alone but also from meteorological data such as atmospheric temperature and wind speed.

Currently, most anthropogenic heat flux studies in remote sensing focus on energy balance models for pure pixels, with no consideration of mixed pixels particularly in heterogeneous urban areas. Although there are some studies that focus on the energy balance of mixed pixels, they are either complex to calculate, which is based on some *a priori* assumptions [11], or require dual-angle satellite images [10]. The work in [22] developed a two-source energy balance model to estimate urban heat fluxes and to analyze the sensitivities of the model parameters; however, this model may not be able to separate anthropogenic heat discharges from the sensible heat fluxes. Typically, most of the remote sensors only provide single-angle observation data; hence, there is a need to develop an accurate and novel algorithm to estimate the anthropogenic heat flux for mixed pixels and to provide the measurements of the anthropogenic heat discharge in urbanized areas with single-angle satellite observations.

Manuscript received October 7, 2014; revised December 14, 2014 and February 5, 2015; accepted February 24, 2015. This work was supported in part by the Research Grants Council of Hong Kong through the Early Career Scheme under Grant F-PP1Q and through the Collaborative Research Fund under Grant HKU9/CRF/12G and in part by the Hong Kong Polytechnic University under Grant G-YM85 and through the Research Institute for Sustainable Urban Development under Grant 1-ZVBR.

M. S. Wong, J. Yang, and J. Nichol are with the Department of Land Surveying and Geo-Informatics, Faculty of Construction and Environment, The Hong Kong Polytechnic University, Kowloon, Hong Kong (e-mail: lswong@polyu.edu.hk; jinxin.yang@connect.polyu.hk; lsjanet@polyu.edu.hk).

Q. Weng is with the Center for Urban and Environmental Change, Indiana State University, Terre Haute, IN 47809-1902 USA (e-mail: qweng@indstate.edu).

M. Menenti is with the Delft University of Technology, 2628 CD Delft, Netherlands (e-mail: m.menenti@tudelft.nl).

P. W. Chan is with Hong Kong Observatory, Kowloon, Hong Kong (e-mail: pwchan@hko.gov.hk).

Color versions of one or more of the figures in this paper are available online at http://ieeexplore.ieee.org.

Digital Object Identifier 10.1109/LGRS.2015.2409111

TABLE I
SPECIFICATIONS OF THE HJ-1B SATELLITE

Sensor	Band	Spectral range (μm)	Spatial resolution (m)	Swath width (km)	Field of view	Revisit time
CCD	1	0.43-0.52	30	360*2	31°	4 days
	2	0.52-0.60				
	3	0.63-0.69				
	4	0.76-0.9				
IRS	1	0.75-1.10	150	720	29°	4 days
	2	1.55-1.75				
	3	3.50-3.90				
	4	10.5-12.5	300			

II. DATA USED AND STUDY AREA

The HJ-1A/B Chinese small satellite launched on September 6, 2008 is used for disaster and environment monitoring. It is a Chinese national project supported by the Ministry of Environmental Protection and the National Committee for Disaster Reduction. The HJ-1A and HJ-1B satellites are on sun-synchronous orbits at the altitude of 650 km. The HJ-1A satellite is equipped with two charge-coupled device (CCD) cameras and a hyperspectral optical camera, whereas the HJ-1B is equipped with the same CCD cameras and one infrared scanner (IRS). The specifications of the HJ-1B are shown in Table I. In this letter, two days of HJ-1B satellite images (October 11, 2012 and January 13, 2013) representing autumn and winter seasons, respectively, were acquired to estimate the anthropogenic heat fluxes of Hong Kong. The territory-wide airborne LiDAR data acquired between December 2010 and January 2011, covering the land areas of the whole territory of Hong Kong, were used in this letter to generate the shadow and sunlit conditions when the satellite overpassed. The land-use data of Hong Kong were also used for the heat flux calculations and the analysis of results.

In addition, the meteorological model data such as air temperature, wind speed, atmospheric pressure, and relative humidity from the Hong Kong Observatory meteorological forecast model at a 120 m altitude and a 2 km spatial resolution, and the global solar radiation measured at a ground station were acquired and used for modeling. In order to calculate the net radiation, the solar radiation was simulated using the Santa Barbara DISORT Atmospheric Radiative Transfer (SBDART) model, and the input parameters were obtained from the AERONET station of Sheung Shui, Hong Kong. The asymmetry factor, the water vapor content, the single-scattering albedo, and the aerosol optical thickness (AOT) from the AERONET station were input into the SBDART model to simulate the direct and diffuse solar radiations. The solar radiation on October 11, 2012 at 10:40 A.M. local time was simulated. The total radiation obtained, the direct solar radiation, and the diffuse solar radiation were 751.69, 460.02, and 291.97 W/m^2, respectively. In comparison, the total solar radiation from the King's Park station measured by the Hong Kong Observatory was 752 W/m^2 at 10:40 A.M. local time. For January 13, 2013, the simulated total solar radiation, the direct radiation, and the diffuse radiation were 540.6, 237.56, and 303.05 W/m^2, respectively.

In this letter, the original radiance images with a 300 m spatial resolution were first converted to "at-satellite" blackbody temperature. Then, the blackbody temperature images were corrected for the emissivity differences of earth materials at a 30 m spatial resolution. This emissivity modulation method enhanced the temperature images to a higher spatial resolution based on the Stefan–Boltzmann law, where the equation is expressed as follows [26]:

$$T_b = \varepsilon^{\frac{1}{4}}(T_s) \tag{1}$$

where T_s is the derived land-surface temperature of the HJ-1B, T_b is the blackbody temperature at 300 m, and ε is the emissivity derived from an image with a 30 m spatial resolution; thus, there are 100 emissivity values at a 300 m resolution. This letter then derived the land-surface temperatures based on the emissivity values at 30 m.

III. METHODOLOGY

In this letter, an advanced and novel anthropogenic heat flux algorithm using the Chinese small satellite HJ-1B is proposed for developing a heat energy balance model for heterogeneous urban areas. The proposed energy balance model can decompose the heat flux from an impervious surface and vegetation within mixed pixels as follows:

$$R_n + A = H_{\text{veg\_imp}} + f * LE_{\text{veg}} + (1-f) * LE_{\text{imp}} + f * G_{\text{veg}} + (1-f) * G_{\text{imp}} \tag{2}$$

where f is the fraction of the vegetation cover that can be calculated by [1]

$$f = \left(\frac{\text{NDVI} - \text{NDVI}_{\min}}{\text{NDVI}_{\max} - \text{NDVI}_{\min}}\right)^2 \tag{3}$$

where NDVI is the Normalized Difference Vegetation Index; $\text{NDVI}_{\min}$ and $\text{NDVI}_{\max}$ can be selected as the lower and upper NDVI values, respectively, e.g., 3% limits from the frequency distribution of all NDVI values; and R_n is the total net radiation of both the vegetation and the impervious surface, and it can be calculated by

$$R_n = (1-\alpha)(\Phi * R_{\text{dir}} + V R_{\text{dif}}) + V\varepsilon\varepsilon_a R_{L\downarrow} - \varepsilon R_{L\uparrow} \tag{4}$$

where Φ is the sunlit fraction in the pixel; V is the sky view factor, which can be calculated by the digital surface model data in Hong Kong; R_{dir} is the direct solar radiation; and R_{dif} is the diffused solar radiation by the atmosphere. The diffuse solar radiation, as opposed to the direct solar radiation, can be simulated in the shadow areas. R_{dir} and R_{dif} can be simulated using the SBDART code with the inputs of the asymmetry factor, the water vapor content, the single-scattering albedo, and the AOT from the AERONET station in Hong Kong. $R_{L\downarrow}$ and $R_{L\uparrow}$ are the downward and upward blackbody radiations that can be calculated by $R_{L\downarrow} = \sigma T_a^4$ and $R_{L\uparrow} = \sigma T_s^4$, respectively [24]; σ is the Stefan–Boltzmann constant; T_a and T_s are the air and surface temperatures, respectively; α is the surface albedo that can be derived from the HJ-1B visible channels; ε is the surface emissivity that can be derived from the land-use map; and ε_a is the atmospheric emissivity that can be estimated from

$$H_{\text{veg\_imp}} = \rho C_p \frac{T_s - T_a}{(f * r_{a\_\text{veg}} + (1-f) * r_{a\_\text{imp}}) + (f * r_{a\_\text{veg}} + (1-f) * r_{e\_\text{imp}})} \tag{5}$$

the empirical equation of the atmospheric water vapor pressure and the atmospheric temperature [4], [22].

For single-observation-angle satellite data, e.g., the HJ-1B, it is challenging to separate the component temperatures of the vegetation and the impervious surface in the mixed pixels. In order to resolve the problem of mixed pixels, the effective resistance was calculated in (5), shown at the top of the page, where $H_{\text{veg\_imp}}$ is the sensible heat flux from the vegetation and the impervious surface. In (5), ρ is the air density; C_p is the specific heat of air at a constant pressure; T_s is the surface temperature from the HJ-1B thermal infrared data; T_a is the atmospheric temperature; and r_{a_veg} and r_{a_imp} are the aerodynamic resistances for the vegetation and the impervious surface, respectively. They can be calculated from the land-use and land-cover data and the high-resolution airborne LiDAR data as follows:

$$r_a = \frac{\ln\left(\frac{z_u - d_0}{z_{0m}}\right) \ln\left(\frac{z_t - d_0}{z_{0h}}\right)}{k^2 u} \tag{6}$$

where Z_u and Z_t are the heights of the wind speed and the atmospheric temperature, respectively; d_0 is the displacement height; and Z_{0m} and Z_{0h} are the roughness lengths for the momentum and the heat transport, respectively. k is von Karman's constant ($= 0.4$), and u is the wind speed. The Z_{0m} and Z_{0h} of different land-use classes can be referred to the work in [4], and r_{e_veg} and r_{e_imp} are the radiometric excess resistances of the vegetation and the impervious surface as follows:

$$r_e = \frac{kB^{-1}}{ku^*} \tag{7}$$

where $kB^{-1} = \ln(z_{0m}/z_{0h})$, and u^* is the friction velocity, i.e.,

$$u^* = uk\left[\ln\left(\frac{z_u - d_0}{z_{0m}}\right) + \psi_m\left(\frac{z_u - d_0}{L}\right) - \psi_m\left(\frac{z_{0m}}{L}\right)\right] \tag{8}$$

where ψ_m is the stability correction function that depends on L, i.e., the Monin–Obukhov length. ψ_m can be deemed as 0 under neutral stratification.

LE_{veg} and LE_{imp} are the latent heat fluxes for the vegetation and the impervious surface, respectively, i.e.,

$$LE_{\text{veg}} = \frac{\rho C_p}{\gamma} \frac{e_s^* - e_a}{r_{a\_\text{veg}} + r_{s\_\text{veg}}}$$
$$LE_{\text{imp}} = \frac{\rho C_p}{\gamma} \frac{e_s^* - e_a}{r_{a\_\text{imp}} + r_{s\_\text{imp}}} \tag{9}$$

where e_s is the saturation water vapor pressure; e_a is the atmospheric water vapor pressure; γ is the psychrometric constant; r_{s_veg} and r_{s_imp} are the stomatal resistances of the vegetation and the impervious surface, respectively; and LE_{imp} tends to be zero in a dry midday. For the vegetation, the stomatal resistance can be referred to the work in [8]. The impervious resistance can be derived from the following [18]:

$$r_{s\_\text{imp}} = \exp(8.206 - 4.255 W_1) \tag{10}$$

where W_1 is the wetness of the 0–5 cm layer. For the impervious surface, W_1 is 0, and the resistance of the impervious surface is 3662.862 s/m.

G_{veg} and G_{imp} are the ground heat fluxes for the vegetation and the impervious surface, respectively, where G_{veg} tends to be zero, and C_{g_imp} and C_{g_veg} are fixed constants based on land-use types as follows [22]:

$$G_{\text{veg}} = C_{g\_\text{veg}} R_n \qquad G_{\text{imp}} = C_{g\_\text{imp}} R_n. \tag{11}$$

Thus, the anthropogenic heat discharge (A) for both pure and mixed pixels can be calculated using the proposed model [see (2)].

IV. Results

A. Heat Fluxes in Hong Kong

The net radiation, the ground heat, the latent heat, the sensible heat, and the anthropogenic heat flux are illustrated in Fig. 1, which shows the derived effective heat fluxes for both pure and mixed pixels at a 30 m spatial resolution. The results show that 99% of the net radiations range from 450 to 680 W/m^2 on October 11, 2012 and from 250 to 477 W/m^2 on January 13, 2013, resulting in average net radiations of 573.9 and 336.2 W/m^2, respectively. In the shadow areas, the shortwave radiation is contributed by the diffuse solar radiation from the sky and by the reflection from neighboring pixels. The latent heat fluxes in urban areas are very low, i.e., only about 5 to 10 W/m^2 on October 11, 2012 and about 3 to 8.75 W/m^2 on January 13, 2013. Both of the (LE/R_n) ratios in urban areas on these two days are very low, and the mean values of the (LE/R_n) ratios are 0.042 and 0.051 on October 11, 2012 and January 13, 2013, respectively. The ratios are similar to the value 0.04 observed in the capital of Mexico in the winter season [14], where most of the land-cover types are impervious surfaces. In the mountainous areas, the latent heat fluxes are much higher than in urban areas, i.e., approximately 50–170 W/m^2 on October 11, 2012 and 25–80 W/m^2 on January 13, 2013, which are close to the latent heat observed in a forest and a grassland in autumn and winter [22]. However, the ground heat fluxes of the vegetation are relatively low, the average of the ground heat fluxes of urban areas are around 259.6 and 211.86 W/m^2 [see Fig. 1(c) and (d)], and the (G_n/R_n) ratio is 0.45 on October 11, 2012, which is similar to the value (0.4) observed in [23], and is 0.63 on January 13, 2013, which is similar to the value (0.58) reported in [14]. The averages of the sensible heat fluxes in urban areas are 474.59 and 294.71 W/m^2 on October 11, 2012 and January 13, 2013, respectively. However, the sensible heat fluxes can reach over 1000 W/m^2 in the central business districts, which is even higher than the net radiation in urban areas. This is mainly due to the additional heat sources of the anthropogenic heat. The anthropogenic heat fluxes in October are much higher than those in January. The averages of the anthropogenic heat fluxes are 289.16 and 283.17 W/m^2 on October 11, 2012 and January 13, 2013, respectively. However, the largest anthropogenic heat

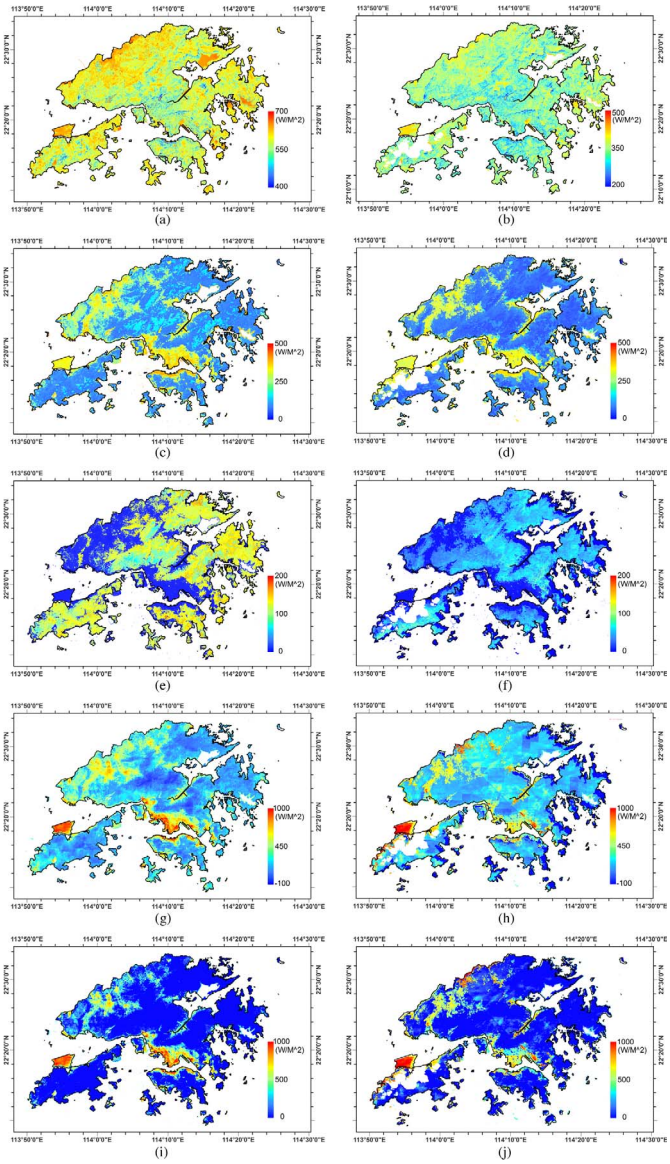

Fig. 1. Different fluxes covering the Hong Kong territories. (a), (c), (e), (g), and (i) Net radiation, ground heat, latent heat, sensible heat, and anthropogenic heat, respectively, on October 11, 2012. (b), (d), (f), (h), and (j) Net radiation, ground heat, latent heat, sensible heat, and anthropogenic heat, respectively, on January 13, 2013.

discharges are observed in particular districts, e.g., Mong Kok in Kowloon Peninsula and the Hong Kong International Airport [see Fig. 1(i) and (j)], and almost reach 800–1000 W/m^2.

B. Correlation of Anthropogenic Heat and Urban Morphology

Figs. 2 and 3 show the relationships of the mean anthropogenic heat fluxes with the building height and the building density. The correlation coefficients between the anthropogenic heat and the building height are 0.58 and 0.62 for October 11, 2012 and January 13, 2013, respectively, when the interval of the building height is defined as 10 m (e.g., the mean anthropogenic heat is calculated at the 0.1 intervals of the building height) (see Fig. 2). The correlation coefficients between the anthropogenic heat and the building density are 0.92 and 0.94 for October 11, 2012 and January 13, 2013, respectively, when the interval of the building density is defined as 0.1 (e.g., the

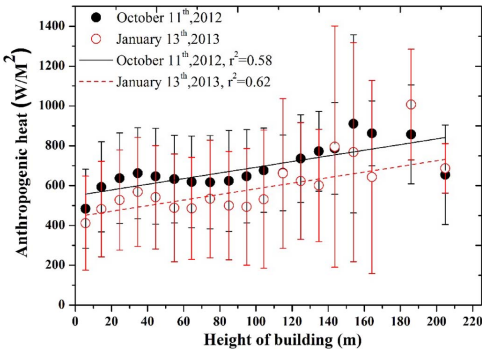

Fig. 2. Relationship of the anthropogenic heat with the building height.

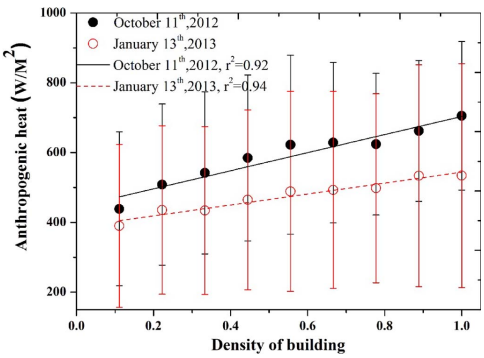

Fig. 3. Relationship of the anthropogenic heat with the density of buildings.

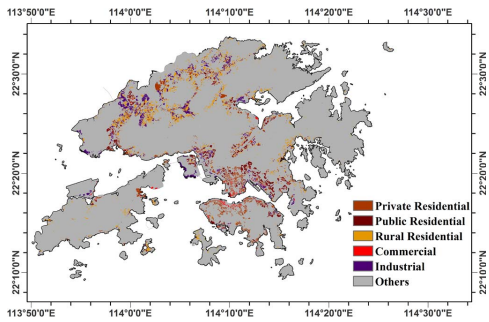

Fig. 4. Land cover and land use in Hong Kong in 2012.

mean anthropogenic heat is calculated at the 0.1 intervals of the building density) (see Fig. 3). Figs. 2 and 3 show that the anthropogenic heat fluxes increase with the building height and the building density, although the trend fluctuates at the building height from 40 to 60 m. The height of buildings and the density of buildings have strong correlations with the anthropogenic heat, which are mainly due to high-rise buildings and the high density of buildings consuming more heating or cooling energy. Another reason is that the height of buildings and the density of buildings have strong influence on the displacement height (d_0), which is highly correlated with sensible heat fluxes in urban areas [22]. Fig. 4 shows the land use and land cover in Hong Kong in 2012. Fig. 5 shows the mean values of the anthropogenic heat in different land uses. The results show that commercial areas have the largest mean anthropogenic heat, i.e., as high as 609.04 and 517.3 W/m^2 on October 11, 2012 and January 13, 2013, respectively. The rural settlement areas have the lowest anthropogenic heat, i.e., 166.2 and 154.7 W/m^2 on October 11, 2012 and January 13, 2013, respectively.

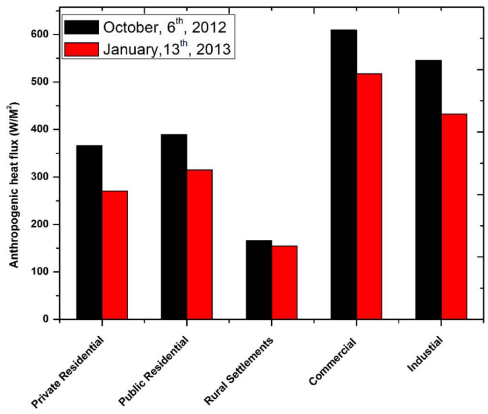

Fig. 5. Comparison of the mean values of the anthropogenic heat fluxes on the two dates.

V. Summary and Conclusion

In this letter, a novel methodology for estimating the anthropogenic heat flux of mixed pixels in heterogeneous urban areas using a single thermal wavelength satellite image has been developed. The heat fluxes calculated by the newly developed method have shown strong relationships to the expected urban anthropogenic cooling and heat patterns. The results show that anthropogenic heat fluxes in Hong Kong are highly correlated with the building density and the building height, with $r^2 = 0.92$ and 0.58 in autumn and $r^2 = 0.94$ and 0.62 in winter, which indicate that high-rise buildings and the high density of buildings may consume more energy for heating or cooling and emit more anthropogenic heat fluxes [19], have higher absorption of irradiance and higher dissipation [12], and have larger dissipation by rougher surfaces with larger aerodynamic roughness. The averages of the anthropogenic heat fluxes in urban areas are 289.16 and 283.17 W/m^2 on October 11, 2012 and on January 13, 2013, respectively. The anthropogenic heat fluxes emitted by commercial areas are the highest among the land-use types. The results and the developed method can be used in planning and environmental authorities to pinpoint "hot-spot" areas of anthropogenic heat, can help in understanding its relation and formation with the UHI effect, and can be used for compliance monitoring. Further work on developing a spatiotemporal adaptive algorithm for anthropogenic heat estimation will be conducted in the near future.

Acknowledgment

The authors would like to thank the Hong Kong Civil Engineering and Development Department for the airborne LiDAR data and the Hong Kong Planning Department for the land-use and land-cover data.

References

[1] R. R. Gillies, W. P. Kustas, and K. S. Humes, "A verification of the 'triangle' method for obtaining surface soil water content and energy fluxes from remote measurements of the normalized difference vegetation index (NDVI) and surface e," *Int. J. Remote Sens.*, vol. 18, no. 15, pp. 3145–3166.

[2] C. Grimmond, "Progress in measuring and observing the urban atmosphere," *Theoret. Appl. Climatol.*, vol. 84, no. 1–3, pp. 3–22, 2006.

[3] T. Ichinose, K. Shimodozono, and K. Hanaki, "Impact of anthropogenic heat on urban climate in Tokyo," *Atmos. Environ.*, vol. 33, no. 24, pp. 3897–3909, Oct. 1999.

[4] S. Kato and Y. Yamaguchi, "Analysis of urban heat-island effect using ASTER and ETM+ data: Separation of anthropogenic heat discharge and natural heat radiation from sensible heat flux," *Remote Sens. Environ.*, vol. 99, no. 1/2, pp. 44–54, Nov. 2005.

[5] S. Kato and Y. Yamaguchi, "Estimation of storage heat flux in an urban area using ASTER data," *Remote Sens. Environ.*, vol. 110, no. 1, pp. 1–17, Sep. 2007.

[6] K. Kłysik, "Spatial and seasonal distribution of anthropogenic heat emissions in Lodz, Poland," *Atmos. Environ.*, vol. 30, no. 20, pp. 3397–3404, Oct. 1996.

[7] S.-H. Lee, C.-K. Song, J.-J. Baik, and S.-U. Park, "Estimation of anthropogenic heat emission in the Gyeong-In region of Korea," *Theoret. Appl. Climatol.*, vol. 96, no. 3/4, pp. 291–303, May 2009.

[8] Q. Mu, M. Zhao, and S. W. Running, "Improvements to a MODIS global terrestrial evapotranspiration algorithm," *Remote Sens. Environ.*, vol. 115, no. 8, pp. 1781–1800, Aug. 2011.

[9] J. E. Nichol, "A GIS-based approach to microclimate monitoring in Singapore's high-rise housing estates," *Photogramm. Eng. Remote Sens.*, vol. 60, no. 10, pp. 1225–1232, 1994.

[10] J. Norman, W. Kustas, J. Prueger, and G. Diak, "Surface flux estimation using radiometric temperature: A dual-temperature-difference method to minimize measurement errors," *Water Resour. Res.*, vol. 36, no. 8, pp. 2263–2274, Aug. 2000.

[11] J. M. Norman, W. P. Kustas, and K. S. Humes, "Source approach for estimating soil and vegetation energy fluxes in observations of directional radiometric surface temperature," *Agric. Forest Meteorol.*, vol. 77, no. 3/4, pp. 263–293, Dec. 1995.

[12] T. R. Oke, "The energetic basis of the urban heat island," *Q. J. R. Meteorol. Soc.*, vol. 108, no. 455, pp. 1–24, Jan. 1982.

[13] T. R. Oke, "Street design and urban canopy layer climate," *Energy Buildings*, vol. 11, no. 1, pp. 103–113, Mar. 1988.

[14] T. R. Oke, R. A. Spronken-Smith, E. Jáuregui, and C. S. B. Grimmond, "The energy balance of central Mexico City during the dry season," *Atmos. Environ.*, vol. 33, no. 24/25, pp. 3919–3930, Oct. 1999.

[15] M. Roth, T. Oke, and W. Emery, "Satellite-derived urban heat islands from three coastal cities and the utilization of such data in urban climatology," *Int. J. Remote Sens.*, vol. 10, no. 11, pp. 1699–1720, 1989.

[16] D. J. Sailor and L. Lu, "A top-down methodology for developing diurnal and seasonal anthropogenic heating profiles for urban areas," *Atmos. Environ.*, vol. 38, no. 17, pp. 2737–2748, 2004.

[17] T. J. Schmugge, W. P. Kustas, and K. S. Humes, "Monitoring land surface fluxes using ASTER observations," *IEEE Trans. Geosci. Remote Sens.*, vol. 36, no. 5, pp. 1421–1430, Sep. 1998.

[18] P. J. Sellers, M. D. Heiser, and F. G. Hall, "Relations between surface conductance and spectral vegetation indices at intermediate (100 m^2 to 15 km^2) length scales," *J. Geophys. Res., Atmos. (1984–2012)*, vol. 97, no. D17, pp. 19 033–19 059, Nov. 1992.

[19] P. Shahmohamadi, A. Che-Ani, A. Ramly, K. Maulud, and M. Mohd-Nor, "Reducing urban heat island effects: A systematic review to achieve energy consumption balance," *Int. J. Phys. Sci.*, vol. 5, no. 6, pp. 626–636, 2010.

[20] R. A. Spronken-Smith, "Comparison of summer-and winter-time suburban energy fluxes in Christchurch, New Zealand," *Int. J. Climatol.*, vol. 22, no. 8, pp. 979–992, 2002.

[21] H. Taha, "Urban climates and heat islands: Albedo, evapotranspiration, and anthropogenic heat," *Energy Buildings*, vol. 25, no. 2, pp. 99–103, 1997.

[22] Q. Weng and P. Fu, "Modeling annual parameters of clear-sky land surface temperature variations and evaluating the impact of cloud cover using time series of Landsat TIR data," *Remote Sens. Environ.*, vol. 140, 267–278, Jan. 2014.

[23] Q. Weng, X. Hu, D. A. Quattrochi, and H. Liu, "Assessing intra-urban surface energy fluxes using remotely sensed ASTER imagery and routine meteorological data: A case study in Indianapolis, USA," *IEEE J. Sel. Topics Appl. Earth Observ. Remote Sens.*, vol. 7, no. 10, pp. 4046–4057, Oct. 2014.

[24] W. Xu, M. Wooster, and C. Grimmond, "Modelling of urban sensible heat flux at multiple spatial scales: A demonstration using airborne hyperspectral imagery of Shanghai and a temperature-emissivity separation approach," *Remote Sens. Environ.*, vol. 112, no. 9, pp. 3493–3510, Sep. 2008.

[25] X. Zhang, Y. Aono, and N. Monji, "Spatial variability of urban surface heat fluxes estimated from Landsat TM data under summer and winter conditions," *J. Agric. Meteorol.*, vol. 54, no. 1, pp. 1–11, 1998.

[26] J. E. Nichol, "An emissivity modulation method for spatial enhancement of thermal satellite images in urban heat island analysis," *Photogram. Eng. Remote Sensing*, vol. 75, no. 5, pp. 547–556, 2009.